Title: Instability in the geological regulation of Earth's climate

Authors: Dominik Hülse[1,2]*,†, Andy Ridgwell[1]*†

Affiliations:

[1]Department of Earth & Planetary Sciences, University of California, Riverside; Riverside, CA 92521

[2]Max-Planck-Institute for Meteorology, Hamburg, Germany

*Corresponding author. Email: dominik.huelse@gmx.de; andy@seao2.org

† Both authors contributed equally.

Abstract: Negative feedback between climate and atmospheric CO_2, as mediated via weathering of silicate minerals, is thought to provide the dominant regulation of Earth's climate on geological timescales. In contrast, we show here that faster feedbacks involving organic matter are critical and create unexpected instability in the system. Specifically, using an Earth system model, we show how organic carbon burial, amplified by climate-sensitive phosphorus feedbacks, can dominate over silicate weathering, inducing a cooling 'over-shoot' and, paradoxically, an ice age in response to massive CO_2 release. This instability in the Earth system is most strongly expressed in the model at intermediate redox states of the ocean and atmosphere, offering a novel explanation for the occurrence of past 'snowball' climates as the Earth's surface became appreciably oxygenated.

One-Sentence Summary: Organic carbon burial, supercharged by climate-sensitive phosphorous feedbacks, can turn warming events into ice ages.

Main Text: Negative feedback must help regulate Earth's climate on geological timescales (here: ca. 100,000 years or more), otherwise even small imbalances between rates of mantle carbon (C) input and removal from the ocean-atmosphere-biosphere system would inexorably lead to unbounded warming (excess input) or cooling (excess removal) *(1, 2)*. The principal stabilizing mechanism is widely assumed to derive from: (i) the climate-sensitive weathering rate of (Ca and Mg-bearing) silicate minerals at the Earth's surface and the associated removal of CO_2 from the atmosphere, and (ii) the atmospheric-CO_2 sensitivity of surface climate – together known as the 'silicate weathering feedback' (*3, 4*; Fig. 1). The response of such a self-regulating system to an initial perturbation, such as the injection of CO_2 into the atmosphere and associated induced climate warming, is a monotonic decrease in the partial pressure of CO_2 in the atmosphere (pCO_2) and cooling back towards the baseline (pre-perturbation) state of climate and global carbon cycling. This decrease in pCO_2 is driven by a well-studied sequence of ocean geochemical and marine sedimentary processes, with silicate weathering being the ultimate (slowest) sink for excess CO_2, operating on a model-estimated timescale of ca. 200 – 300 kyr *(5,6)*. Terrestrial silicate weathering feedback (together with the alteration of oceanic basalts via subsurface circulation of seawater *(7, 8)*) should have been active and provided stabilizing feedback on climate since the inception of plate tectonics on Earth *(9)*. However, the episodic occurrence of extreme cooling and 'snowball Earth' events *(10,11)* and massive organic matter deposition in response to warming events (e.g., *12*), suggests that additional processes are required to fully understand the regulation of climate on geological timescales.

As life evolved on Earth, carbon capture by CO_2 reaction with silicate rocks and subsequent removal by carbon burial in the form of calcium (and magnesium) carbonates ($CaCO_3$) in marine sediments was supplemented by carbon removal in the ocean (and later, at the land surface) in the form of organic matter, i.e., carbon fixed by photo- (or chemo-) synthesis which escapes bacterial degradation to be buried in accumulating sediments *(13)*. Although organic matter burial is modulated by temperature and oxygen together with the mineralogy and accumulation rates of other sediment phases *(14)*, ultimately, nutrient availability and the total rate of biological primary productivity that can be supported must exert overall control *(13, 15)*. Here we focus on the global cycle of phosphorus (P) *(16 – 18)*, both as a principal component of the control of organic matter production, as well as providing additional feedback with climate. Firstly, as is the case for silicate minerals, the weathering rate of phosphorus-bearing minerals such as apatite (together with a lesser contribution from kerogens (ancient organic matter)) is climate-sensitive *(19, 20)*. In the absence of limitation by additional nutrients (fixed nitrogen, dissolved iron), higher rates of P weathering and supply to the ocean will support enhanced rates of primary production and hence organic carbon (C_{org}) burial in marine sediments – a negative feedback on climate (Fig. 1). Secondly, increased seafloor de-oxygenation, driven by increased organic matter production and remineralization, will promote PO_4^{3-} regeneration from the sediments *(21)*. The resulting increased oceanic PO_4^{3-} inventory will further increase primary production in a positive feedback, which in turn, and critical to this study, amplifies the C_{org} burial negative feedback on climate (Fig. 1).

That these feedbacks operate is supported by the geological record of events such as 'Ocean Anoxic Event 2' (OAE2) – a severe carbon cycle and climate perturbation during the Cretaceous at ~93 Ma. OAE2 follows an interval of elevated volcanism and CO_2 release and is characterized by the global occurrence of black shales *(12)* (indicating enhanced C_{org} burial) together with anomalously high sedimentary (organic) C/P ratios *(22)* (indicating enhanced PO_4^{3-} regeneration). However, while the potential role of the organic matter sub-system in climate recovery has previously been explored in numerical modeling of specific events such as OAE2 *(23)*, transient warming at the Paleocene-Eocene boundary (the Paleocene-Eocene Thermal Maximum – 'PETM') *(24)*, and cooling associated with Late Ordovician glaciation *(25)*, missing has been a full appreciation of how this leads to a very different underlying dynamic to the geological regulation of Earth's climate as does silicate weathering alone.

With a series of numerical experiments using the cGENIE 'muffin' Earth system model *(26)*, we illustrate how the evolution of life and progressive surface oxygenation of the Earth paradoxically gives rise to climate instability rather than increasingly robust regulation. We configure the model (Materials and Methods) using an idealized continental arrangement (so as to be independent of any particular time in Earth's history). We include the set of inorganic (CO_2 consumption via silicate weathering plus $CaCO_3$ preservation in marine sediments) and organic (CO_2 and PO_4^{3-} release via kerogen and apatite (P-only) weathering on land plus parameterizations of C_{org} and P preservation in marine sediments) global carbon cycle processes that together constitute the primary long-term feedbacks with climate (as outlined above). In a first set of model experiments (see Table 1), we isolate different combinations of C and P feedbacks to illustrate which processes promote climate destabilization as opposed to stabilization (results of all possible feedback combinations are given in SM). Our second set of experiments takes the form of a limited (4x4) gridded parameter ensemble over which we vary the initial strength of the marine biological pump and atmospheric pO_2 to explore how the relative strengths of key feedbacks may have varied through Earth's history. All experiments (both series) are run for a total of 400 kyr starting from a common initial steady state (from 1112 μatm, Materials and Methods) and are perturbed by a total release of 10,000 PgC, which is released evenly over the first 10 kyr of the simulation (i.e., 1 PgC yr^{-1}) – comparable to inferred rates associated with well-studied past events such as the PETM *(24)* and the end-Permian mass extinction *(27)*.

Isolating different carbon and phosphorus feedbacks

We start by illustrating the consequences of a 'classic' silicate-weathering-only response to perturbation (e.g., as per *(5, 6)*) – experiment 'fixedCwCbPwPb' (Table 1). The model simulates a peak pCO_2 value of 4068 μatm at the end of the 10 kyr interval of CO_2 emissions, after which, and as expected from previous studies, there is a simple monotonic decline (here reaching 1317 μatm by 400 kyr) (Fig. 2a). In contrast, if we add organic carbon weathering and C_{org} burial to silicate weathering and $CaCO_3$ burial ('fixedPwPb'), we obtain runaway greenhouse warming. This is because CO_2 released from kerogen weathering provides a positive feedback that is stronger than the negative silicate weathering feedback, while the global rate of C_{org} burial (and the related negative feedback on climate) responds only weakly (Fig. 2h). However, two notable changes occur if we add responsive P weathering and burial to complete the set of all feedbacks encoded in the model ('fixedNONE'), as illustrated in Fig. 1. Firstly, pCO_2 decreases much faster following the end of carbon emissions than in the silicate-weathering-only scenario ('fixedCwCbPwPb'). Secondly, and unexpectedly, pCO_2 overshoots the initial value some 80 kyr into the experiment to create a cooler climate than in the initial state and with more expansive sea-ice cover (Fig. 2a, b, c). This 'over-cooling' persists for ~150 kyr until pCO_2 and climate rebound back above the initial state, creating a damped oscillatory response to the perturbation. Damped oscillatory responses are not unexpected in systems with multiple interacting feedbacks and have been seen in mathematical representations of the interaction between ice sheet dynamics and carbon cycling *(28)* as well as, more, recently in ocean circulation models *(29)*.

We note that with all feedbacks activated, climate instability exists even in the corresponding control experiment in which there is no CO_2 release or explicit initial perturbation (SM, Fig. S3).

Our findings do not qualitatively depend on the assumption that the global carbon kerogen weathering flux is significant and/or climate-dependent. For instance, comparing experiments 'fixedCw' (invariant kerogen weathering) and 'fixedNONE' demonstrates that adding a positive kerogen weathering CO_2 feedback in the latter configuration only leads to a slightly longer-lasting initial interval of elevated pCO_2 (Fig. 2a). This, in turn, further increases the total (time-integrated) weathering supply of P to the ocean (Fig. 2d, 2f) and hence ultimately amplifies the magnitude of climate over-cooling by a further 1.7°C (Fig. 2b). Testing additional combinations of feedbacks reveals that an initial warming-induced increase in the oceanic PO_4^{3-} inventory from weathering is a pre-requisite to activating strong positive P (and negative C_{org} burial) feedbacks (contrast 'fixedPw' vs. 'fixedNONE'). Conversely, fixing P burial ('fixedPb') prevents the oceanic PO_4^{3-} inventory from ever returning to its initial value. In this scenario, continuously elevated biological productivity and C_{org} burial eventually induce a fully ice-covered snowball state in the model (Fig. 2).

The possibility of over-cooling in response to a warming trigger is also evident in the model results of Papadomanolaki et al. *(23)*, who simulate transient global carbon cycle dynamics across OAE2. Although OAE2 is widely recognized to be an initially volcanism-driven warming event, an abrupt temperature drop of ca. 4 – 11°C occurred during the recovery interval of black shale deposition and elevated carbon isotopic composition ($\delta^{13}C$, *(30, 31)*) – the so-called Plenus Cold Event. A transient cooling episode, characterized by elevated C_{org} burial and $\delta^{13}C$, during recovery is qualitatively consistent with our model findings (Fig. 2h, i). Although the box model used by Papadomanolaki et al. *(23)* (LOSCAR-P; *(32)*) differs from our model in resolution and whether climate dynamics (e.g., ocean circulation) and feedbacks (e.g., sea-ice extent) are accounted for, it includes comparable representations of the same key C and P feedback processes. This leads us to conclude that the critical combination of C and P feedbacks enables over-cooling and, furthermore, that this is an inherent and fundamental property of the Earth system. To increase confidence in our inference, we additionally repeat the main perturbation experiments (Table 1) but with a very different idealized continental arrangement and substitute a mechanistic, oxygen- and burial-rate-dependent representation of C_{org} preservation *(33)* in place of the empirical schemes (Materials and Methods). We find an almost identical dynamical response (SM).

Quantifying feedback strength over Earth history

Critically, the key feedbacks we identify are not invariant through geological time. Because (a) terrestrial weathering responds to changes in continental configuration and evolutionary innovations in land plants *(34)*, and (b) sedimentary P-regeneration is sensitive to the oxygenation state of the ocean (and atmosphere) *(18, 21)*, the relative strengths of the feedbacks and hence how climate is regulated, will have changed as the Earth surface evolved. To illustrate this, we consider all feedbacks acting together but now change their relative strengths. We do this by initializing the model with different plausible boundary conditions spanning at least the past ca. 600 million years. Specifically, we explore variability in (i) atmospheric oxygen (pO_2, in the range: x0.4 to x1.0 modern (0.21 atm)) and (ii) ocean PO_4^{3-} inventory (range: x0.6 to x1.2 modern (2.1 μmol kg^{-1})). Variability in pO_2 is chosen to modulate P burial rates via the influence of ocean oxygenation on the fraction of PO_4^{3-} that is regenerated *(21)* (this also has a minor secondary impact on C_{org} burial). Whereas changes in [PO_4^{3-}], by controlling biological export, modulates both C_{org} and P_{org} burial rates (as well as seafloor oxygenation and hence PO_4^{3-}

regeneration). The 16 parameter combinations of initial pO_2 vs. $[PO_4^{3-}]$ create a wide range of steady-state C_{org} and P burial rates (Fig. 3a, b), P residence times (Fig. 3c), and hence feedback strengths. We then run the same 400 kyr-long carbon perturbation experiments as before (plus controls). Note that we do not aim to simulate the long-term evolution of atmospheric oxygen itself in these experiments, although atmospheric pO_2 can evolve in our simulations in response to changes in organic carbon burial.

For each member of the model parameter ensemble, we summarize the response as the difference between the initial value of pCO_2 (~1112 μatm) and the minimum value reached at any time following the end of the 10 kyr interval of carbon emissions (Fig. 3d, full experimental time series are given in SM). In this analysis, a small positive value is consistent with a monotonic decrease of atmospheric CO_2 back towards (but not yet reaching) the baseline state (i.e., a classic silicate weathering feedback response), whereas a negative value indicates cooling over-shoot. Fig. 3e shows at what time during the experiment the post-emissions pCO_2 minimum occurs. Different stability regimes become apparent, with higher initial ocean $[PO_4^{3-}]$ generally tending to amplify the cooling over-shoot (Fig. 3d), while higher atmospheric pO_2 accelerates climate recovery (Fig. 3e). A 'sweet spot' occurs for a combination of intermediate pO_2 in conjunction with modern or slightly elevated $[PO_4^{3-}]$, when pCO_2 falls below preindustrial (278 ppm, i.e., a negative deviation of ≥850 μatm – ensemble members #7, #8, #12 in Fig. 3d). These 'glaciation' experiments correspond to high rates of C_{org} but only intermediate P burial (Fig. 3f).

At low initial atmospheric pO_2 in our model, P regeneration is already close to its maximum limit (and sedimentary C/P is far higher than 'Redfield', Fig. S6d), which, in conjunction with a long P residence time (Fig. 3c) supports only weak positive P feedback. The linked negative C_{org} burial feedback (Fig. 1) is hence also weak, resulting in only gradual and mild over-cooling (#1 – #4, Fig. 3d, e). In contrast, at high pO_2 (#14 – #16), sedimentary C/P is initially low and close to Redfield (Fig. S6d), while P burial (and weathering) is elevated. The resulting short P residence time, in conjunction with only a weak P regeneration response, due to initially well-oxygenated conditions, enables ocean PO_4^{3-} to be efficiently restored back to pre-perturbation concentrations (SM, Fig. S4v, x), leading to rapid but only mild over-cooling (Fig. 3d, e). The choice of initial ocean PO_4^{3-} concentration exerts a more predictable overall control, with faster and more intense over-cooling generally scaling with PO_4^{3-} inventory. As noted, intense ice ages ('snowballs') occur in the model under relatively high ocean PO_4^{3-} inventories but only under intermediate states of ocean (and atmosphere) oxygenation (#7, #8, #12; Fig. 3d, e), which we suggest offers a novel insight into the climate history of Earth.

Implications for Earth's climate regulation

Two episodes of global-scale glaciation are known from the geological record: the Huronian glaciations during the Paleoproterozoic (2.45 - 2.22 Ga *(35, 36)*) and then during the late Neoproterozoic, the Sturtian (onset 717.5 to 716.3 Ma *(37)*) and Marinoan glaciation (onset 649.9 to 639.0 Ma *(37)*). Likewise, the history of atmospheric oxygen is characterized by two primary transitions. The first – the 'Great Oxygenation Event'– occurred 2.5-2.3 Ga *(38)*, thus approximately coincident with (or closely preceding) the first Huronian glaciation *(39)*, and could have seen pO_2 climb towards present-day values before dropping back down. The second rise in oxygenation back again towards more modern-like values occurred between ~800 - 540 Ma and was thus closely associated in time with the Sturtian and Marinoan *(37, 38)*. Previous authors have linked the occurrence of glaciation and oxygenation via the highly redox-sensitive methane (CH_4) cycle and greenhouse forcing *(40, 41)* or entirely oxygen-independent mechanisms such as carbon drawdown from the silicate weathering of fresh basalts associated with Rodinia breakup *(42, 43)*. While not exclusive of other mechanisms, we propose that changes in atmospheric oxygen are indeed central to a 'snowball Earth' event, but that glaciation occurs as a consequence of extreme instability in climate regulation under intermediate oxygenation states. As in our idealized modeling in which we induced P-cycle feedbacks and glaciation (over-cooling) via an initial release of CO_2 to the atmosphere, both global-scale glacial episodes have been associated with the emplacement of large igneous provinces (LIPs) that could have acted as an initial trigger: (i) the Huronian glaciation by a series of LIP events *(44)* and (ii) the Sturtian glaciation by the Franklin LIP *(45)*. However, in our model, ice ages could be triggered by other mechanisms resulting in the enhanced phosphate delivery to the ocean *(18, 25, 46)* with the magnitude of the cooling determined by the initial state of global C and P cycling (Fig. 3). The absence of extreme glaciation prior to 2.45 Ga, during the later Paleoproterozoic and Mesoproterozoic, and later during the Phanerozoic, can be explained as a consequence of atmospheric oxygen being either too low or too high to support sufficiently strong feedbacks and hence climatic instability.

We do not expect the specific values of pO_2 at which extreme over-cooling arises in the model – the 'sweet spot' interval in Fig. 3 – to necessarily correspond to values inferred from the geological record (e.g., *(38)*). The cGENIE 'muffin' Earth system model as used here is relatively low in spatial resolution, adopts an idealized continental configuration, and lacks dynamically coupled atmosphere and ice sheets. We also employ relatively simple global average and/or empirically based formulations for key P and C feedbacks (see Methods), and omit consideration of possible Fe and N co-limitations. Changing any of these assumptions might narrow or expand the 'sweet spot' interval and/or shift to lower or higher values of pO_2. However, the existence of comparable results generated with different continental configurations and feedback formulations (SM), as well as the over-cooling observed in box modeling of OAE2 *(23)*, leads us to conclude that the phenomena is real and provides a single simple interpretative framework for the occurrence of global-scale glaciation.

Finally, we point out that a classic silicate-weathering-dominated response occurs only under low PO_4^{3-} and close-to-modern pO_2 (#9, #13). For present-day ocean phosphate, and with key weathering and burial fluxes within the uncertainty of present-day estimates (Fig. 3f), we obtain mild over-cooling that starts about 70 kyr following the cessation of emissions (Fig. 2). Hence, rather than continued fossil fuel carbon release causing a persistent atmospheric CO_2 burden that could delay the next glacial inception by 100-400 kyr or more *(6, 47, 48)*, the 'long tail' of elevated CO_2 *(49)* may not be quite so long after all. The underappreciated role of the organic matter sub-system in the Earth system in facilitating much more rapid future CO_2 drawdown than widely assumed (e.g., *(50)*) could yet allow for orbitally-triggered glacial inception within 50-70 kyr from now *(48)*.

References and Notes

1. J. F. Kasting, Long-term stability of the earth's climate. *Global and Planetary Change* **1**, 83-95 (1989).
2. R. A. Berner, K. Caldeira, The need for mass balance and feedback in the geochemical carbon cycle. *Geology* **25**, 955 (1997).
3. 3. J. C. G. Walker, P. B. Hays, J. F. Kasting, A negative feedback mechanism for the long-term stabilization of Earth's surface temperature. *Journal of Geophysical Research* **86**, 9776 (1981).
4. 4. R. A. Berner, A. C. Lasaga, R. M. Garrels, The carbonate-silicate geochemical cycle and its effect on atmospheric carbon dioxide over the past 100 million years. *American Journal of Science* **283**, 641-683 (1983).
5. 5. D. Archer, H. Kheshgi, E. Maier-Reimer, Multiple timescales for neutralization of fossil fuel CO2. *Geophysical Research Letters* **24**, 405-408 (1997).
6. 6. N. S. Lord, A. Ridgwell, M. C. Thorne, D. J. Lunt, An impulse response function for the "long tail" of excess atmospheric CO2 in an Earth system model. *Global Biogeochemical Cycles* **30**, 2-17 (2016).
7. K. Caldeira, Long-term control of atmospheric carbon dioxide; low-temperature seafloor alteration or terrestrial silicate-rock weathering? *American Journal of Science* **295**, 1077-1114 (1995).
8. L. A. Coogan, S. E. Dosso, Alteration of ocean crust provides a strong temperature dependent feedback on the geological carbon cycle and is a primary driver of the Sr-isotopic composition of seawater. *Earth and Planetary Science Letters* **415**, 38-46 (2015).
9. J. Korenaga, Initiation and Evolution of Plate Tectonics on Earth: Theories and Observations. *Annual Review of Earth and Planetary Sciences* **41**, 117-151 (2013).
10. D. A. Evans, N. J. Beukes, J. L. Kirschvink, Low-latitude glaciation in the Palaeoproterozoic era. *Nature* **386**, 262-266 (1997).
11. P. F. Hoffman, A. J. Kaufman, G. P. Halverson, D. P. Schrag, A Neoproterozoic Snowball Earth. *Science* **281**, 1342-1346 (1998).
12. S. Schlanger, H. Jenkyns, Cretaceous Oceanic Anoxic Events: Causes and Consequences. *Geologie en Mijnbouw* **55**, 3-4 (1976).
13. D. J. Burdige, Preservation of Organic Matter in Marine Sediments: Controls, Mechanisms, and an Imbalance in Sediment Organic Carbon Budgets? *Chemical Reviews* **107**, 467-485 (2007).
14. M. J. Kennedy, D. R. Pevear, R. J. Hill, Mineral Surface Control of Organic Carbon in Black Shale. *Science* **295**, 657-660 (2002).
15. T. F. Pedersen, S. E. Calvert, Anoxia vs. Productivity: What Controls the Formation of Organic-Carbon-Rich Sediments and Sedimentary Rocks? *AAPG Bulletin* **74**, 454-466 (1990).
16. T. Tyrrell, The relative influences of nitrogen and phosphorus on oceanic primary production. *Nature* **400**, 525-531 (1999).

17. K. Wallmann, Phosphorus imbalance in the global ocean? *Global Biogeochemical Cycles* **24**, GB4030 (2010).
18. C. T. Reinhard, et al., Evolution of the global phosphorus cycle. *Nature* **541**, 386-389 (2017).
19. M. W. Guidry, F. T. Mackenzie, Apatite weathering and the Phanerozoic phosphorus cycle. *Geology* **28**, 631-634 (2000).
20. E. W. Bolton, R. A. Berner, S. T. Petsch, The Weathering of Sedimentary Organic Matter as a Control on Atmospheric O2: II. Theoretical Modeling. *American Journal of Science* **306**, 575-615 (2006).
21. E. Ingall, R. Jahnke, Evidence for enhanced phosphorus regeneration from marine sediments overlain by oxygen depleted waters. *Geochimica et Cosmochimica Acta* **58**, 2571-2575 (1994).
22. H. P. Mort, et al., Phosphorus and the roles of productivity and nutrient recycling during oceanic anoxic event 2. *Geology* **35**, 483-486 (2007).
23. N. M. Papadomanolaki, N. A. van Helmond, H. Pälike, A. Sluijs, C. P. Slomp, Quantifying volcanism and organic carbon burial across Oceanic Anoxic Event 2. *Geology* **50**, 511-515 (2022).
24. M. Gutjahr, et al., Very large release of mostly volcanic carbon during the Palaeocene–Eocene Thermal Maximum. *Nature* **548**, 573-577 (2017).
25. J. Longman, B. J. W. Mills, H. R. Manners, T. M. Gernon, M. R. Palmer, Late Ordovician climate change and extinctions driven by elevated volcanic nutrient supply. *Nature Geoscience* **14**, 924-929 (2021).
26. A. Ridgwell, J. C. Hargreaves, Regulation of atmospheric CO2 by deep-sea sediments in an Earth system model. *Global Biogeochemical Cycles* **21**, GB2008 (2007).
27. Y. Wu, et al., Volcanic CO2 degassing postdates thermogenic carbon emission during the end-Permian mass extinction. *Science Advances* **9**, eabq4082 (2023).
28. J. C. Zachos, L. R. Kump, Carbon cycle feedbacks and the initiation of Antarctic glaciation in the earliest Oligocene. *Global and Planetary Change* **47**, 51-66 (2005).
29. A. Pohl, et al., Continental configuration controls ocean oxygenation during the Phanerozoic. *Nature* **608**, 523-527 (2022).
30. M. M. M. Kuypers, R. D. Pancost, J. S. S. Damsté, A large and abrupt fall in atmospheric CO2 concentration during Cretaceous times. *Nature* **399**, 342-345 (1999).
31. J. S. Sinninghe Damsté, E. C. van Bentum, G.-J. Reichart, J. Pross, S. Schouten, A CO2 decrease-driven cooling and increased latitudinal temperature gradient during the mid-Cretaceous Oceanic Anoxic Event 2. *Earth and Planetary Science Letters* **293**, 97-103 (2010).
32. N. Komar, R. E. Zeebe, Redox-controlled carbon and phosphorus burial: A mechanism for enhanced organic carbon sequestration during the PETM. *Earth and Planetary Science Letters* **479**, 71-82 (2017).
33. D. Hülse, S. Arndt, S. Daines, P. Regnier, A. Ridgwell, OMEN-SED 1.0: a novel, numerically efficient organic matter sediment diagenesis module for coupling to Earth system models. *Geosci. Model Dev.* **11**, 2649-2689 (2018).

34. T. M. Lenton, M. Crouch, M. Johnson, N. Pires, L. Dolan, First plants cooled the Ordovician. *Nature Geoscience* **5**, 86-89 (2012).

35. D. Zakharov, et al., Dating the Paleoproterozoic snowball Earth glaciations using contemporaneous subglacial hydrothermal systems. *Geology* **45**, 667-670 (2017).

36. A. Bekker, "Huronian Glaciation" in *Encyclopedia of Astrobiology*, M. Gargaud, et al., eds. (Springer, Berlin, Heidelberg, 2015), pp. 1128–1135.

37. P. F. Hoffman, et al., Snowball Earth climate dynamics and Cryogenian geology-geobiology. *Science Advances* **3**, e1600983 (2017).

38. T. W. Lyons, C. T. Reinhard, N. J. Planavsky, The rise of oxygen in Earth's early ocean and atmosphere. *Nature* **506**, 307-315 (2014).

39. M. R. Warke, et al., The Great Oxidation Event preceded a Paleoproterozoic "snowball Earth". *Proceedings of the National Academy of Sciences* **117**, 13314-13320 (2020).

40. K. Zahnle, M. Claire, D. Catling, The loss of mass-independent fractionation in sulfur due to a Palaeoproterozoic collapse of atmospheric methane. *Geobiology* **4**, 271-283 (2006).

41. D. P. Schrag, R. A. Berner, P. F. Hoffman, G. P. Halverson, On the initiation of a snowball Earth. *Geochemistry, Geophysics, Geosystems* **3**, 1-21 (2002).

42. Y. Donnadieu, Y. Goddéris, G. Ramstein, A. Nédélec, J. Meert, A 'snowball Earth' climate triggered by continental break-up through changes in runoff. *Nature* **428**, 303-306 (2004).

43. Y. Goddéris, et al., The Sturtian 'snowball' glaciation: fire and ice. *Earth and Planetary Science Letters* **211**, 1-12 (2003).

44. A. P. Gumsley, et al., Timing and tempo of the Great Oxidation Event. *Proceedings of the National Academy of Sciences* **114**, 1811-1816 (2017).

45. J. P. Pu, et al., Emplacement of the Franklin large igneous province and initiation of the Sturtian Snowball Earth. *Science Advances* **8**, eadc9430 (2022).

46. L. J. Alcott, B. J. W. Mills, A. Bekker, S. W. Poulton, Earth's Great Oxidation Event facilitated by the rise of sedimentary phosphorus recycling. *Nature Geoscience* **15**, 210-215 (2022).

47. D. Archer, A. Ganopolski, A movable trigger: Fossil fuel CO2 and the onset of the next glaciation. *Geochemistry, Geophysics, Geosystems* **6**, Q05003 (2005).

48. A. Ganopolski, R. Winkelmann, H. J. Schellnhuber, Critical insolation–CO2 relation for diagnosing past and future glacial inception. *Nature* **529**, 200-203 (2016).

49. D. Archer, Fate of fossil fuel CO2 in geologic time. *Journal of Geophysical Research: Oceans* **110**, C09S05 (2005).

50. J. E. Tierney, et al., Past climates inform our future. *Science* **370**, eaay3701 (2020).

51. A. Ridgwell, et al., Marine geochemical data assimilation in an efficient Earth System Model of global biogeochemical cycling. *Biogeosciences* **4**, 87-104 (2007).

52. G. Colbourn, A. Ridgwell, T. M. Lenton, The Rock Geochemical Model (RokGeM) v0.9. *Geosci. Model Dev.* **6**, 1543–1573 (2013).

53. P. Vervoort, S. Kirtland Turner, F. Rochholz, A. Ridgwell, Earth System Model Analysis of How Astronomical Forcing Is Imprinted Onto the Marine Geological Record: The Role of the Inorganic (Carbonate) Carbon Cycle and Feedbacks. *Paleoceanography and Paleoclimatology* **36**, e2020PA004090 (2021).

54. M. D. Iglesias-Rodriguez, et al., Progress made in study of ocean's calcium carbonate budget. *Eos, Transactions American Geophysical Union* **83**, 365-375 (2002).

55. N. A. O'Mara, J. P. Dunne, Hot Spots of Carbon and Alkalinity Cycling in the Coastal Oceans. *Scientific Reports* **9**, 4434 (2019).

56. C. T. Hayes, et al., Global Ocean Sediment Composition and Burial Flux in the Deep Sea. *Global Biogeochemical Cycles* **35**, e2020GB006769 (2021).

57. J. A. Bradley, D. Hülse, D. E. LaRowe, S. Arndt, Transfer efficiency of organic carbon in marine sediments. *Nature Communications* **13**, 7297 (2022).

58. J. P. Dunne, J. L. Sarmiento, A. Gnanadesikan, A synthesis of global particle export from the surface ocean and cycling through the ocean interior and on the seafloor. *Global Biogeochemical Cycles* **21**, GB4006 (2007).

59. C. R. Benitez-Nelson, The biogeochemical cycling of phosphorus in marine systems. *Earth-Science Reviews* **51**, 109-135 (2000).

60. K. C. Ruttenberg, "8.13 - The Global Phosphorus Cycle" in *Treatise on Geochemistry*, H. D. Holland, K. K. Turekian, eds. (Pergamon, Oxford, 2003), pp. 585–643.

61. R. E. Zeebe, T. Tyrrell, History of carbonate ion concentration over the last 100 million years II: Revised calculations and new data. *Geochimica et Cosmochimica Acta* **257**, 373-392 (2019).

62. C. P. Slomp, E. H. G. Epping, W. Helder, W. V. Raaphorst, A key role for iron-bound phosphorus in authigenic apatite formation in North Atlantic continental platform sediments. *Journal of Marine Research* **54**, 1179-1205 (1996).

63. E. D. Ingall, R. M. Bustin, P. Van Cappellen, Influence of water column anoxia on the burial and preservation of carbon and phosphorus in marine shales. *Geochimica et Cosmochimica Acta* **57**, 303-316 (1993).

64. E. Ingall, R. Jahnke, Influence of water-column anoxia on the elemental fractionation of carbon and phosphorus during sediment diagenesis. *Marine Geology* **139**, 219-229 (1997).

65. C. P. Slomp, J. Thomson, G. J. de Lange, Enhanced regeneration of phosphorus during formation of the most recent eastern Mediterranean sapropel (S1). *Geochimica et Cosmochimica Acta* **66**, 1171-1184 (2002).

66. T. J. Algeo, E. Ingall, Sedimentary Corg:P ratios, paleocean ventilation, and Phanerozoic atmospheric pO2. *Palaeogeography, Palaeoclimatology, Palaeoecology* **256**, 130-155 (2007).

67. R. A. Wildman, et al., The weathering of sedimentary organic matter as a control on atmospheric O2: I. Analysis of a black shale. *American Journal of Science* **304**, 234-249 (2004).

68. R. G. Hilton, A. J. West, Mountains, erosion and the carbon cycle. *Nature Reviews Earth & Environment* **1**, 284-299 (2020).

69. R. A. Berner, GEOCARBSULF: A combined model for Phanerozoic atmospheric O2 and CO2. *Geochimica et Cosmochimica Acta* **70**, 5653-5664 (2006).

70. J. Gaillardet, B. Dupré, P. Louvat, C. J. Allègre, Global silicate weathering and CO2 consumption rates deduced from the chemistry of large rivers. *Chemical Geology* **159**, 3-30 (1999).

71. W. Ludwig, P. Amiotte-Suchet, J.-L. Probst, Enhanced chemical weathering of rocks during the last glacial maximum: a sink for atmospheric CO2? *Chemical Geology* **159**, 147-161 (1999).

72. G. Munhoven, Glacial–interglacial changes of continental weathering: estimates of the related CO2 and HCO_3^- flux variations and their uncertainties. *Global and Planetary Change* **33**, 155-176 (2002).

73. F. E. Muller-Karger, et al., The importance of continental margins in the global carbon cycle. *Geophysical Research Letters* **32** (2005).

74. R. A. Berner, *Early Diagenesis: A Theoretical Approach* (Princeton University Press, 1980).

75. D. E. Canfield, Factors influencing organic carbon preservation in marine sediments. *Chemical Geology* **114**, 315–329 (1994).

76. D. E. LaRowe, P. Van Cappellen, Degradation of natural organic matter: A thermodynamic analysis. *Geochimica et Cosmochimica Acta* **75**, 2030-2042 (2011).

Acknowledgments:

Funding:

Simons Postdoctoral Fellowships in Marine Microbial Ecology (award 653829) (DH)

National Science Foundation grant EAR-2121165 (AR)

NASA Interdisciplinary Consortia for Astrobiology Research (ICAR) Program (80NSSC21K0594) NASA (AR)

NASA Nexus for Exoplanet System Science (NExSS) and the NASA Exobiology Program (Grant 80NSSC19K0461) (AR)

Author contributions: Conceptualization: DH, AR

Methodology: DH, AR

Investigation: DH, AR

Visualization: DH, AR

Writing: DH, AR

Competing interests: Authors declare that they have no competing interests.

Data and materials availability: The code for the version of the 'muffin' release of the cGENIE Earth system model used in this paper, is tagged as v0.9.40, and is assigned a DOI: 10.5281/zenodo.7714267. Configuration files for the specific experiments presented in the paper can be found in the directory: genie-userconfigs/PUBS/submitted/Huelse_Ridgwell.Science.2023. Details of the experiments, plus the command line needed to run each one, are given in the readme.txt file in that directory. All other configuration files and boundary conditions are provided as part of the code release. A manual detailing code installation, basic model configuration, tutorials covering various aspects of model configuration, experimental design, and output, plus the processing of results, is assigned a DOI: 10.5281/zenodo.7545814.

Supplementary Materials

Materials and Methods

Supplementary Text

Figs. S1 to S8

Table S1

References (*51 – 76*) are only cited in the SM.

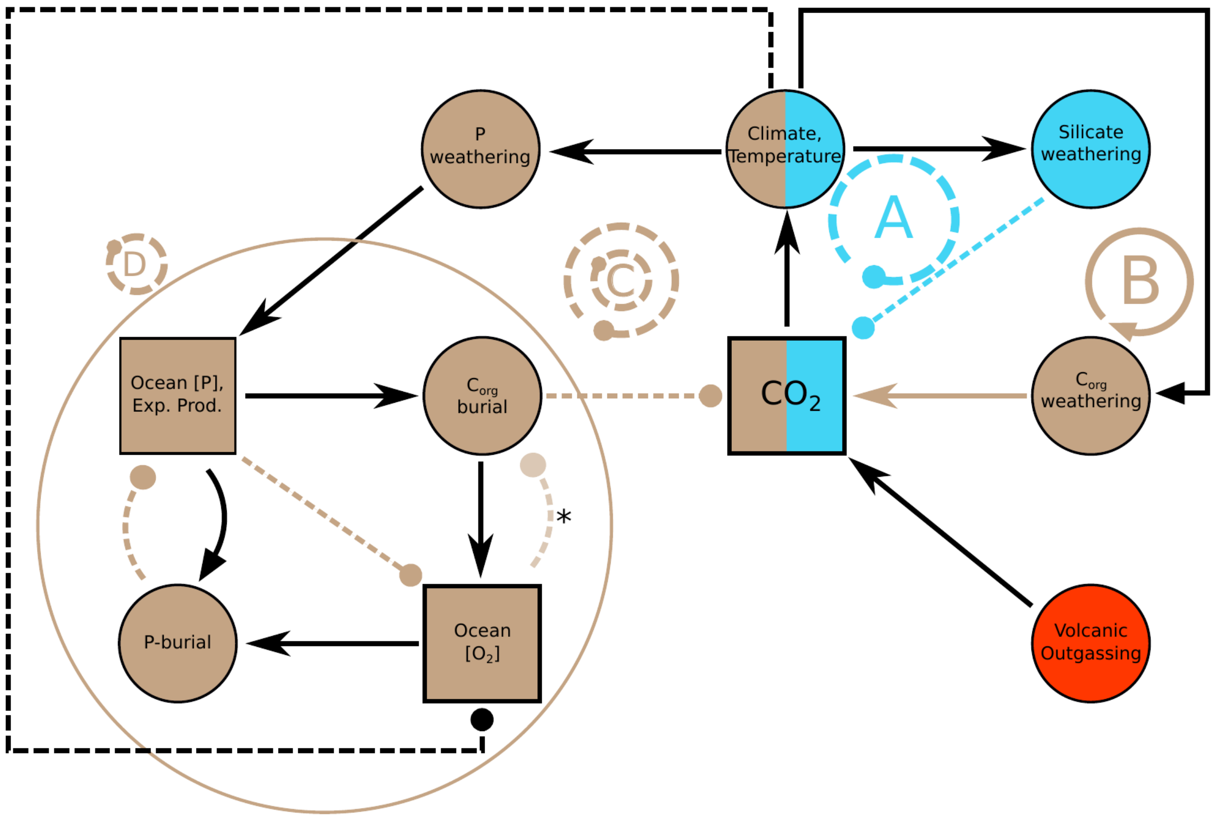

Fig. 1. Schematic of processes and feedback cycles included in the cGENIE model. In blue: Silicate weathering (circle A); Brown: Organic matter sub-system (circles B, C, D); Red: Volcanic outgassing. The organic matter sub-system consists of: The organic carbon (C_{org}) weathering feedback (circle B); the C_{org} burial feedback (circle C); the P cycle feedbacks (circle D) consisting of 3 sub-cycles and getting externally perturbed by P weathering and changes in ocean [O_2] due to temperature changes. Small circular arrows around the letters indicate faster feedbacks and larger circular arrows slower feedbacks. Solid arrows indicate positive feedback, dashed lines with dots indicate negative feedback. *: This effect is only explicitly accounted for in the alternative configuration tested (described in SM).

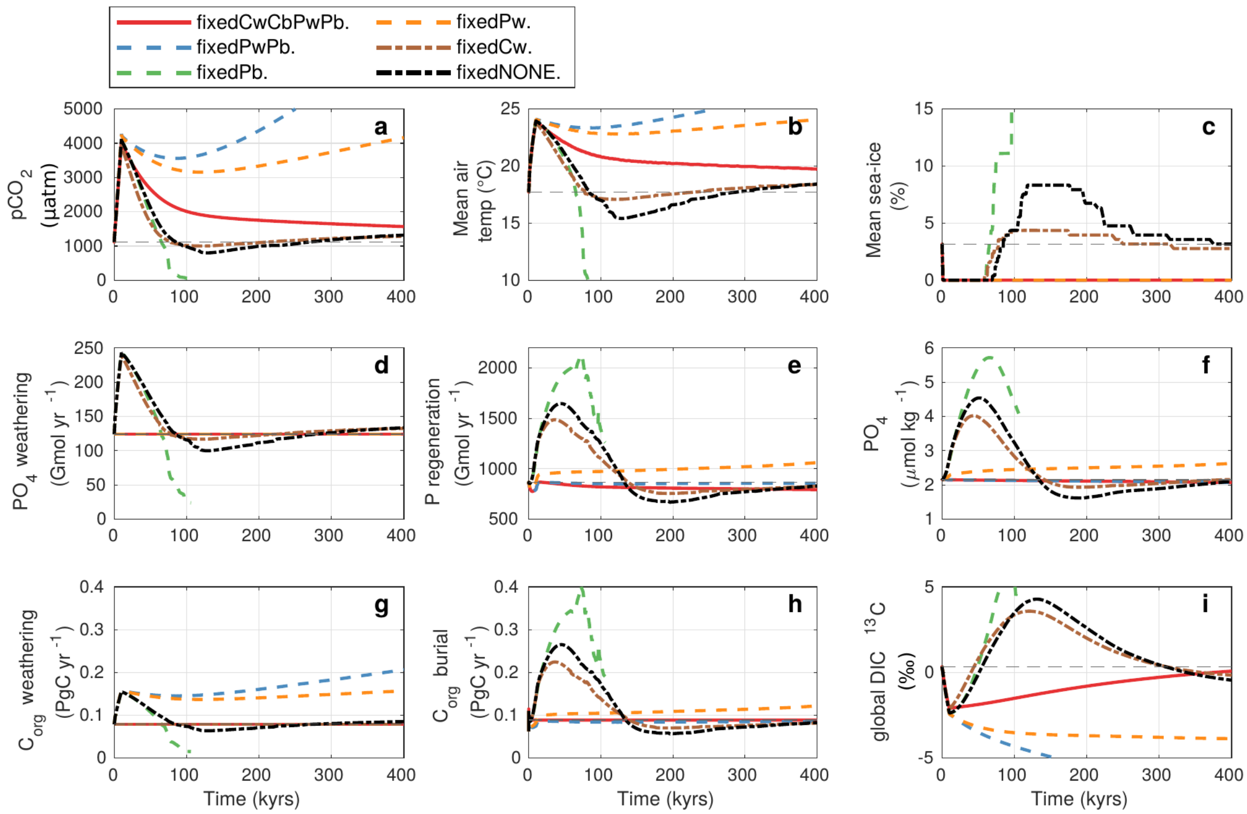

Fig. 2. Time-evolution of the model system in response to perturbation. Time-series plots for the perturbation simulation (CO_2 release of 10,000 PgC over 10 kyr) and the system recovery over 400 kyr for the 'feedback' experiments of Table 1. The horizontal dashed lines indicate the pre-perturbation condition.

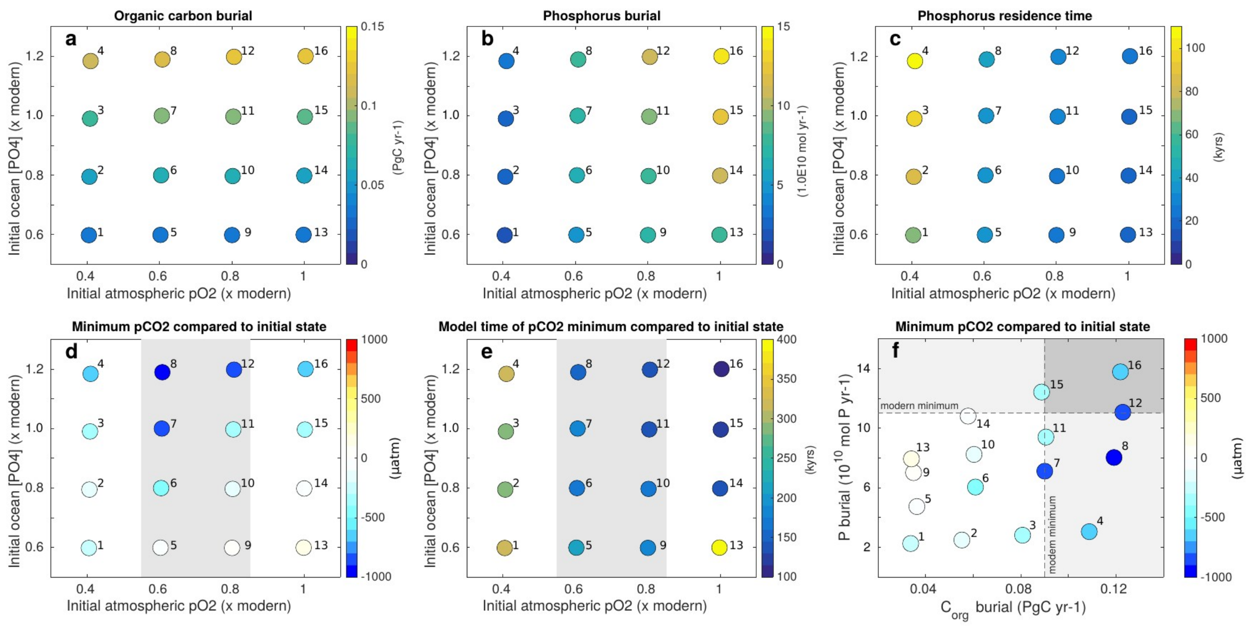

Fig. 3. Analysis of the 16 'Strengths' experiments of Table S1. The panels show steady-state **(a)** global organic carbon burial, **(b)** global P burial and **(c)** P residence time at the end of SPIN2. The pCO$_2$ minimum compared to initial state **(d, f)** and the model time of this minimum **(e)** during the recovery from the climate perturbation. Note the different x- and y-axis in f. Grey areas in d+e illustrate the 'sweet spot' interval of intermediate pO2. Grey areas in f show ranges for estimated modern Corg and P burial fluxes (see Fig. S1 for values and references). (Fig. S6 includes the scalar values for a-e.)

Table 1: Overview of the 'feedbacks' experiments shown in Fig. 2. For all numerical experiments see Table S1.

Experiment Name	Description
fixedCwCbPwPb	Classic silicate-weathering-only: C_{org} and P feedbacks disabled
fixedPwPb	Silicate-weathering + C_{org} feedbacks; P feedbacks (weathering and burial) disabled
fixedPb	Silicate-weathering + C_{org} feedbacks + P-weathering; P burial fixed to equilibrium rate
fixedPw	Silicate-weathering + C_{org} feedbacks + P burial; P-weathering fixed to equilibrium rate
fixedCw	Silicate-weathering + P feedbacks + C_{org} burial; C_{org} weathering fixed to equilibrium rate
fixedNONE	All feedbacks enabled

Science
AAAS

Supplementary Materials for

Instability in the geological regulation of Earth's climate

Dominik Hülse*, Andy Ridgwell*

Corresponding author: dominik.huelse@gmx.de; andy@seao2.org

The PDF file includes:

Materials and Methods
Supplementary Text
Figs. S1 to S8
Table S1
References

Material and Methods

Description of the Earth system model cGENIE

cGENIE is an Earth system model of intermediate complexity based on a frictional-geostrophic 3D ocean circulation model which is coupled to a fast energy–moisture balance 2D atmosphere and a dynamic–thermodynamic sea-ice component. cGENIE includes a detailed representation of ocean biogeochemical cycles (*51*) and the long-term (inorganic) carbon cycle is represented through input and removal of dissolved carbon species via terrestrial carbonate and silicate rock weathering (*52*) and the preservation of biogenic calcium carbonates in marine sediments (*26*). The cycling of carbon and associated tracers in the ocean is based on a single (phosphate) nutrient limitation of biological productivity and a double-exponential expression to calculate the particulate organic matter (POM) flux in the water column (*51*). Note that we do not include a temperature-dependent scheme for the remineralization of POM.

cGENIE is implemented on a 18 $\times$ 18 equal-area grid with 14 unevenly spaced vertical levels. We deliberately chose an idealized continental configuration in order to provide a more generalized feedback understanding than would be possible, if we would use a specific configuration. We adopt the configuration of ref. (*53*) where a single continent stretches from pole to pole across all latitudes and a flat-bottom bathymetry with a maximum depth of $\sim$3,575 m is used to approximate the modern ocean volume. We modify the bathymetry of ref. (*53*) by surrounding the continent by a continental shelf with a depth of $\sim$175 m to include shallow water depositional environments (Figure S1a) that are expected to modulate the strength of the organc carbon (C_{org}) and P-cycle feedback. We also apply the random spatial distribution of ocean sediment depths of ref. (*53*) (Figure S1b) that is used in the pressure-dependent calculation of calcium carbonate preservation. Note that we run the same experiments using two additional idealized continental configurations. One configuration with a single super-continent centered in the northern polar region and a second configuration where the continent covers only low latitudes and features an equatorial gateway. Both configurations do not qualitatively change our results (not shown).

Because cGENIE lacks a dynamical atmosphere, we apply the simplified zonally averaged 2D wind speed and wind stress, and 1D zonally averaged albedo forcing fields generated by ref. (*53*), using the 'muffingen' open-source software (https://doi.org/10.5281/zenodo.5500687). We assume global carbon cycle conditions to approximate generic Phanerozoic greenhouse conditions and to prevent both perennial and seasonal seaice formation. Initial values comprise: 1112 μatm atmospheric pCO_2 and -6.5‰ atmospheric $\delta^{13}C$; major ion concentrations of 27.0 mmol kg^{-1} Ca^{2+}, 35.0 mmol kg^{-1} Mg^{2+} and 11.8 mmol kg^{-1} SO_4^{2-} for 100 Ma following Zeebe and Tyrrell (*61*); alkalinity (1983 μmol kg^{-1}) and DIC (2056 μmol kg^{-1}) was chosen to represent a mean ocean concentration corresponding with 1112 μatm pCO_2. A $CaCO_3$/POM export rain ratio of 0.15 in conjunction with mean surface ocean $\Omega = 6.0$ was chosen to give a modern-like mean sediment wt% CaCO3. (Note that we also perform model experiments using preindustrial atmospheric CO_2 concentrations (as described in 'Additional cGENIE simulations') which does not qualitatively change our results.)

Including C_{org} and P feedbacks

To represent feedbacks related to the organic carbon sub-system on longer timescales we include a simple representation for organic carbon burial in the sediments into cGENIE. The approach uses the simple empirically-derived equation of Dunne et al. (*58*):

$$F_{\mathrm{OC_{bur}}} = F_{\mathrm{OC_{set}}} \cdot \left(0.013 + \frac{0.53 \cdot F_{\mathrm{OC_{set}}}^2}{(7.0 + F_{\mathrm{OC_{set}}})^2}\right)$$

Here organic carbon burial, $F_{\mathrm{OC_{bur}}}$, scales with organic matter rain flux to the sediment and is hence a function of surface productivity. Note that we also use a more elaborate representation

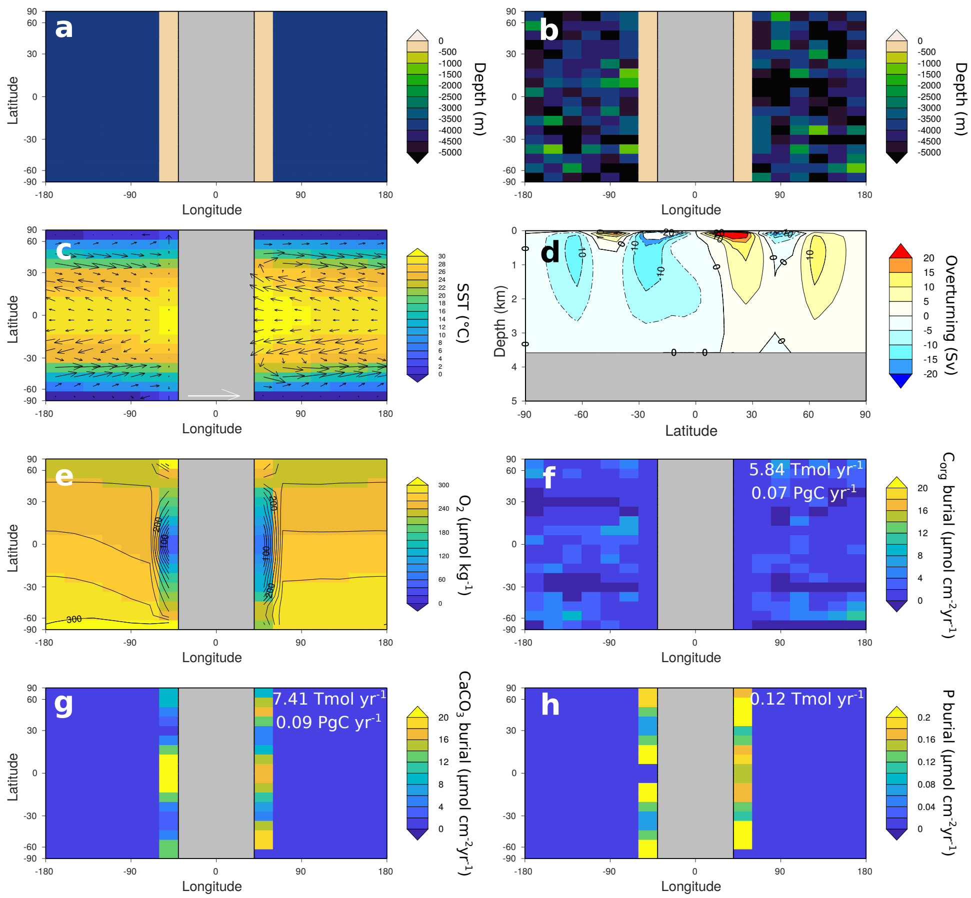

Figure S1: cGENIE configuration and equilibrium boundary conditions at the end of SPIN2. **(a)** Continental configration and flat-ocean bathymetry used in the ocean circulation model. **(b)** Random spatial distribution of ocean depths used in the pressure-dependent calculation of calcium carbonate preservation in the sediments. **(c)** Simulated sea surface temperatures (SST) superimposed by vectors for ocean surface velocities, **(d)** the zonal mean ocean overturning strength, **(e)** seafloor oxygen concentration, and burial rates of **(f)** $CaCO_3$, **(g)** organic carbon, and **(h)** phosphorus in the marine sediments. Comparable modern burial fluxes: $CaCO_3$ = 0.074 - 0.136 PgC yr^{-1} (*54–56*); organic carbon = 0.09 - 0.30 PgC yr^{-1} (*57, 58*); phosphorus = 0.11 - 0.34 Tmol yr^{-1} (*59, 60*).

where organic carbon burial is calculated by an early diagenetic model and degradation rates respond to the bottom water oxygen concentration (see section 'Additional cGENIE experiments' below).

In order to account for redox-dependent P-regeneration from sediments in cGENIE we implemented the empirical parameterization of Wallmann (*17*). A large fraction of the organically bound phosphorus (P_{org}) is degraded in the surface sediments and transformed into dissolved phosphate (PO_4). Some of this PO_4 is recycled back to the water column via molecular diffusion and bioirrigation, while the remaining fraction can absorb to manganese and iron oxides or form authigenic P-bearing silicate minerals, such as apatite (*62*). Measurements of sediment-water interface fluxes, and C:P regeneration and burial ratios show that PO_4 is preferentially released from sediments in low-oxygen environments (*21, 63–66*).

The parameterization of Wallmann - see equation (1) in (*17*) - describes this oxygen dependence of the regeneration ratio (r_{REG}) by calculating the benthic regeneration of PO_4, PO_4^{rt}, as a function of seafloor oxygen concentration, O_2^{sf} (in μmol/kg), and the depth integrated rate of OC degradation in the surface sediments, R_{OC}. We adapted the parameterization of Wallmann (*17*) by assuming that his fitting parameter A corresponds to the C/P ratio of settling POM, $\frac{C}{P}_{\mathrm{rain}} = -\frac{C}{P}$, and then create his fitting parameter Y_F by adding an offset of $o = 11$:

$$r_{\mathrm{REG}} = \frac{R_{\mathrm{OC}}}{\mathrm{PO}_4^{\mathrm{rt}}} = \left(\frac{C}{P}_{\mathrm{rain}} + o\right) - \frac{C}{P}_{\mathrm{rain}} \cdot exp\left(-\frac{O_2^{\mathrm{sf}}}{r}\right)$$

with $r = 32$ as specified in Wallmann (*17*). Hence, in cGENIE, the original fitting parameters Y_F and A vary with C/P of settling POM, and the anoxic C/P value (11.0) is the same as in the original parameterization.

To account for these losses over longer timescales the terrestrial weathering model of cGENIE has been extended with representations for the oxidative weathering of kerogen (i.e., ancient organic matter) and weathering of phosphorous-bearing minerals (e.g., apatite). Kerogen weathering can be represented by the reaction $CH_2O + O_2 \longrightarrow CO_2 + H_2O$ (with organic matter represented in its simple form CH_2O) and thus represents an additional source of CO_2 to the atmosphere. The global weathering fluxes of P and kerogen can either automatically track the burial rates (i.e., creating a closed system in order to create an equilibrium state), or they can follow the same climate sensitivity as silicate- and carbonate-rock weathering. Measurements and modelling work has shown that erosion rate (or errosive stripping) and kerogen concentration in rocks are more important for the oxidative weathering rate than changes in atmospheric pO_2 (*20, 67*). And also more recent work has suggested a link between climate and kerogen weathering (*68*). Thus, following the GEOCARBSULF approach (*69*), we do not include an oxygen dependency of kerogen weathering.

Description of the numerical experiments and diagnostic variables for plotting

cGENIE is equilibrated in a two-step spin-up process analagous to ref. (*26*). In a first stage 20 kyr spin-up (SPIN1) ocean dynamics and ocean biogeochemical cycling equilabrates with the prescribed values of atmospheric pCO_2 and $\delta^{13}C$. This spin-up is run as a closed system, so solutes lost through burial of $CaCO_3$, C_{org} and P are instantaneously restored through global weathering fluxes of carbonates, silicates, kerogen and P. Bioturbation is turned 'off' so an equilibrium state of surface sediment composition and burial rates are achieved faster. We use the results of SPIN1 to diagnose the global equilibrium burial rates of $CaCO_3$, C_{org} and P. The second stage 50 kyr spin-up (SPIN2) is run as an open system (i.e., without prescribing atmospheric pCO_2 and $\delta^{13}C$). Weathering fluxes are set to the global $CaCO_3$, C_{org} and P burial rates diagnosed in SPIN1 and respond to temperature changes. Based on modern continental weathering studies (e.g., (*70–72*)) we assume a 0.6:0.4 carbonate:silicate weathering ratio to balance the global $CaCO_3$ burial. To (isotopically) balance the additional burial of C_{org} we use a combination of CO_2 outgassing and kerogen weathering with an isotopic composition of volcanic CO_2 outgassed of -6.0 ‰. More details on how the weathering parameters are calculated to balance the system can be found in Section *'Mass balance calculations'* below and in the online documentation (see: code availability section). Bioturbation is turned 'on' to simulate more realistic ocean-sediment interactions. The steady-state surface sediment burial fluxes are shown in Figure S1(f, g, h). Our model simulates a mean surface sediment content of 36 wt% and a global burial rate of $CaCO_3$ in deep sea sediments of 0.07 PgC yr^{-1}, thus at the lower end of previous estimates for the modern ocean (i.e., 0.074 - 0.136 PgC yr^{-1} (*54–56*) without coral reefs). Our simulated global C_{org} burial rate is 0.09 PgC yr^{-1} of which 0.084 PgC yr^{-1} are preserved on the continental shelf. Our calculated C_{org} burial rate compares well with recent model estimates for global C_{org} transfer efficiency at 1m sediment depth (i.e., 0.09 Pg C yr^{-1}; (*57*)) and is slightly lower than previous observational estimates for the modern ocean (i.e., 0.15 – 0.30 Pg C yr-1; (*58,73*)). Our global P-burial rate is 0.124 Tmol yr^{-1} and thus at the lower end of previous estimates for the modern ocean (i.e., 0.11 – 0.34 Tmol yr^{-1}, (*59,60*)). Note that in this setup C_{org} burial is slightly larger than $CaCO_3$ burial. We make the opposite assumption (i.e., simulating slightly larger $CaCO_3$ than C_{org} burial) in our additional cGENIE experiments where we use OMEN-SED to calculate C_{org} burial; at the same time we also simulate slightly higher overall C burial fluxes (see Fig. S7 and the related text).

Starting from the equilibrium state, SPIN2, we force the model with a CO_2 release of 10,000 PgC to the atmosphere over 10 kyr and then simulate system recovery over 400 kyr. We assume an isotopic signal of -15‰ for the CO_2 emissions, thus representing a mixture of volcanism and organic carbon. Our emission scenario is meant to represent a generic Phanerozoic carbon cycle perturbation and not a specific event. However, comparable rates are associated with well-studied past events such as the PETM (*24*) and the end-Permian mass extinction (*27*). We run two separate sets of model experiments (plus controls) as summarized in Table S1. With the first set of experiments ('Feedbacks'), we evaluate the system response to disabling various C-P feedbacks. In the second set ('Strengths'), we enable all C-P feedbacks and vary their relative strengths by adjusting the steady-state ocean PO_4^{3-} and atmospheric pO_2 concentration via a small (4×4) gridded parameter ensemble.

The following diagnostic variables are calculated from the model output and plotted in the output Figures S2 and S3 to aid interpretation of the dynamic behavior of the model: Subfigure (k) The fractional C_{org} burial in the sediment is calculated as C_{org} burial flux over C_{org} settling flux. Subfigure (o) The fractional P-regeneration, $FracP^{reg}$, is calculated as the sediment-water interface flux of dissolved P divided by the organic P transfer from the ocean to the sediment, $FPorg^{ocnsed}$). Subfigure (p) We calculate the P-regeneration that is caused by redox changes alone and not by an increased organic P settling flux by assuming that the fractional P-regeneration of SPIN2 ($\widetilde{\mathrm{FracP}}^{\mathrm{reg}}$, i.e., grey dashed horizontal line in (o)) is the steady-state P-regeneration. Hence, we can calculate the redox-dependent P-regeneration over time t as: $\mathrm{Predox}^{\mathrm{reg}}(t) = \left(\mathrm{FracP}^{\mathrm{reg}}(t) - \widetilde{\mathrm{FracP}}^{\mathrm{reg}}\right) \times \mathrm{FPorg}^{\mathrm{ocnsed}}(t)$.

<u>Mass balance calculations</u>

In order to reach a steady-state in our open system spin-ups the carbon losses via $CaCO_3$ and C_{org} need to be balanced. Hence the bulk carbon mass balance that needs to be satisfied in steady-state is:

$$F_{out(Corg)} + F_{out(CaCO3)} = F_{in(CO2)} + F_{in(Corg)} + F_{in(CaCO3)}$$

where $F_{out()}$ are the burial fluxes of organic carbon (C_{org}) and calcium carbonate ($CaCO_3$); $F_{in(Corg)}$ and $F_{in(CaCO3)}$ are the respective weatherig fluxes; and $F_{in(CO2)}$ represents the volcanic CO_2 outgassing flux. Because we also want the system to be isotopically balanced we need to consider the following equation:

$$\delta^{13}C_{out(Corg)} \times F_{out(Corg)} + \delta^{13}C_{out(CaCO3)} \times F_{out(CaCO3)} =$$
$$\delta^{13}C_{in(CO2)} \times F_{in(CO2)} + \delta^{13}C_{in(Corg)} \times F_{in(Corg)} + \delta^{13}C_{in(CaCO3)} \times F_{in(CaCO3)}$$

Table S1: Overview of numerical experiments conducted for this study.

Set 1: 'Feedbacks'	
Experiment Name	Description
fixedCwCbPwPb	Classic silicate-weathering-only: C_{org} and P feedbacks disabled
fixedPwPb	Silicate-weathering + C_{org} feedbacks; P feedbacks (weathering and burial) disabled
fixedPb	Silicate-weathering + C_{org} feedbacks + P-weathering; P burial fixed to equilibrium rate
fixedPw	Silicate-weathering + C_{org} feedbacks + P burial; P-weathering fixed to equilibrium rate
fixedCwCb	Silicate-weathering + P feedbacks; C_{org} burial and weathering fixed to equilibrium rate
fixedCb	Silicate-weathering + P feedbacks + C_{org} weathering; C_{org} burial fixed to equilibrium rate
fixedSlw	C_{org} + P feedbacks + carbonate weathering; silicate-weathering fixed to equilibrium rate
fixedCARBw	C_{org} + P feedbacks + silicate-weathering; carbonate-weathering fixed to equilibrium rate
fixedSlwCARBw	C_{org} + P feedbacks; silicate - and carbonate-weathering fixed to equilibrium rates
fixedCw	Silicate-weathering + P feedbacks + C_{org} burial; C_{org} weathering fixed to equilibrium rate
fixedNONE	All feedbacks enabled
Set 2: 'Strenghts' - all feedbacks enabled	
Variable	Steady-state concentrations
Ocean PO_4^{3-}	0.6, 0.8, 1.0, 1.2 $\times$ default 2.159 μmol kg^{-1}
Atmospheric pO_2	0.4, 0.6, 0.8, 1.0 $\times$ default 0.2095 atm

The latter equation can be simplyfied by assuming that: (i) the isotopic composition of weathered kerogen is the same as newly buried C_{org} ($\delta^{13}C_{out(Corg)}$), and (ii) the isotopic composition of weathered carbonate is the same as newly buried $CaCO_3$ ($\delta^{13}C_{out(CaCO3)}$).[1] Thus resulting the following equation for the isotopic mass balance:

$$\begin{aligned}&\delta^{13}C_{out(Corg)} \times F_{out(Corg)} + \delta^{13}C_{out(CaCO3)} \times F_{out(CaCO3)} = \\ &\delta^{13}C_{in(CO2)} \times F_{in(CO2)} + \delta^{13}C_{out(Corg)} \times F_{in(Corg)} + \delta^{13}C_{out(CaCO3)} \times F_{in(CaCO3)}\end{aligned} \tag{1}$$

Note that the value of $\delta^{13}C_{in(CO2)}$ is prescribed in the model and has a value of $-6‰$. As we assume that $CaCO_3$ burial is balanced by 40% silicate and 60% carbonate weathering (e.g., (*70–72*)) two unknown parameters remain in equation (1): the kerogen weathering flux, $F_{in(Corg)}$, and the volcanic CO_2 outgassing flux, $F_{in(CO2)}$. We can further assume that a fraction, γ, of $F_{in(CO2)}$ partly balances the C_{org} burial flux in addition to balancing silicate weathering. Thus, we have two additonal equations to balance the organic and carbonate carbon burial fluxes:

$$F_{out(Corg)} = \gamma \times F_{in(CO2)} + F_{in(Corg)} \tag{2}$$

$$F_{out(CaCO3)} = (1 - \gamma) \times F_{in(CO2)} + F_{in(CaCO3)} \tag{3}$$

Hence we have 3 equations (1) – (3) with three unknowns (i.e., $F_{in(CO2)}$, $F_{in(Corg)}$, γ). Substituting equations (2) and (3) into (1) and solving for γ gives:

$$\gamma = \frac{\delta^{13}C_{in(CO2)} - \delta^{13}C_{out(CaCO3)}}{\delta^{13}C_{out(Corg)} - \delta^{13}C_{out(CaCO3)}} \tag{4}$$

The values for $\delta^{13}C_{out(Corg)}$ and $\delta^{13}C_{out(CaCO3)}$ are reported as cGENIE output (in sed-diag_misc_DATA_GLOBAL.res). From this we can calculate $F_{in(CO2)}$ and $F_{in(Corg)}$ using equation (3) and (2), respectively.

[1]As a point of reference, the long-term Phanerozoic average value is ca. $2 - 4‰$.

Supplementary Text

Analysis of the perturbation experiments using different feedbacks

Figure S2 shows various physical and biogeochemical state-variables and diagnostics for the 'Feedbacks' experiments of Table S1. The model develops a runaway greenhouse when parts of the organic matter sub-system are considered but either P-weathering or C_{org} burial are fixed (i.e., 'fixedPw', 'fixedPwPb', 'fixedCwCb', 'fixedCb' – ordered by increasing rapidity of the runaway effect). In these experiments silicate weathering either alone ('fixedCwCb', 'fixedCb') or in combination with C_{org} burial ('fixedPw', 'fixedPwPb') does not provide a strong enough negative feedback to bring the system back to the pre-perturbation state. This results because either C_{org} burial can not keep up with the initial CO_2 perturbation ('fixedCwCb'), the positive kerogen weathering feedback is too strong ('fixedCb'), or the oceanic PO_4 inventory (and thus organic matter production, export and C_{org} burial) is not sensitive enough to climate change ('fixedPw', 'fixedPwPb'; see e.g Fig. S2h, i, j).

For all other experiments that acoount for parts of the organic matter sub-system feedbacks a more or less strong over-cooling occurs (i.e., 'fixedCw', 'fixedNONE', 'fixedCARBw', 'fixed-Slw', 'fixedSlwCARBw', 'fixedPb' – ordered by increasing magnitude of the over-cooling, Fig. S2 b). Note in particular that a fixed P burial alone (i.e., a no'fixedPb') prevents the oceanic PO_4^{3-} from returning to its pre-perturbation value. Here, continuesly elevated organic matter production and C_{org} burial (Fig. S2 j, n) eventually results in a fully ice-covered snowball state (Fig. S2 c). The over-cooling effect is stronger when the inorganic feedbacks (silicate and carbonate weathering) are not considered in the model (i.e., 'fixedCARBw', 'fixedSlw', 'fixed-SlwCARBw'; see Fig. S2b). For the classic silicate-weathering only scenario ('fixedCwCbP-wPb') the carbon isotope composition of dissolved inorganic carbon ($\delta^{13}C_{DIC}$) only shows a negative excursion due to the initial perturbation, followed by a linear increase back towards the pre-perturbation value (Fig. S2 l). In contrast, our model simulates elevated $\delta^{13}C_{DIC}$ during the recovery interval when we consider responsive C_{org} burial (and a sensitive oceanic PO_4^{3-} inventory, i.e., all experiments except 'fixedPwPb', 'fixedPw', 'fixedCwCb', 'fixedCb'). The positive carbon isotope excursion is strongest when the silicate-weathering is fixed ('fixedSlw', 'fixedSlwCARBw').

Figure S3 shows the control simulations for all feedback experiments of Table S1 – i.e., the same experiments as shown in Figure S2 but without simulating the CO_2 release.

Analysis of the perturbation experiments pO_2 vs. PO_4 using all C-P feedbacks

Figures S4 and S5 show six biogeochemical state-variables for the 'Strengths' experiments described in Table S1. Under the lowest initial pO_2 conditions (i.e., $pO_2 = 0.4\times$modern, solid lines in Fig. S4 and S5) the P-feedback is weakest as indicated by the low magnitudes of P-weathering and P-burial (e.g., Fig. S4e, f), as well as the very long P-residence times (Fig. S6c). As a result the oceanic PO_4^{3-} inventory and thus C_{org} burial responds comparably weak and slow to the pCO_2 perturbation (Fig. S4c, d). For the $0.4\times pO_2$ experiments the speed of the initial climate recovery inversely scales with the initial ocean PO_4^{3-} inventory (Fig. S4a) and takes longer than in experiments with higher initial pO_2 conditions (compare Fig. S5a, g, m, f). However, also the $0.4\times pO_2$ experiments exhibit over-cooling which starts at $\sim$220 kyrs and its magnitude positively scales with the initial ocean PO_4^{3-} inventory (Fig. S4a).

Under all other pO_2 conditions (i.e., pO_2 of 0.6, 0.8 and 1.0×modern) the rapidity of the initial climate recovery and the size of the over-cooling positively scales with the initial ocean PO_4^{3-} inventory (Fig. S4g, m, s). Climate recovery is fastest for the largest initial pO_2 conditions and the highest nutrient inventory (yellow, dotted lines in Fig. S4 and S5). Surprisingly, however, over-cooling is strongest for experiments starting from intermediate initial pO_2 conditions (i.e., $0.6\times pO_2$ + $1.0\times PO_4^{3-}$, $0.6\times pO_2$ + $1.2\times PO_4^{3-}$, $0.8\times pO_2$ + $1.2\times PO_4^{3-}$). Here, the

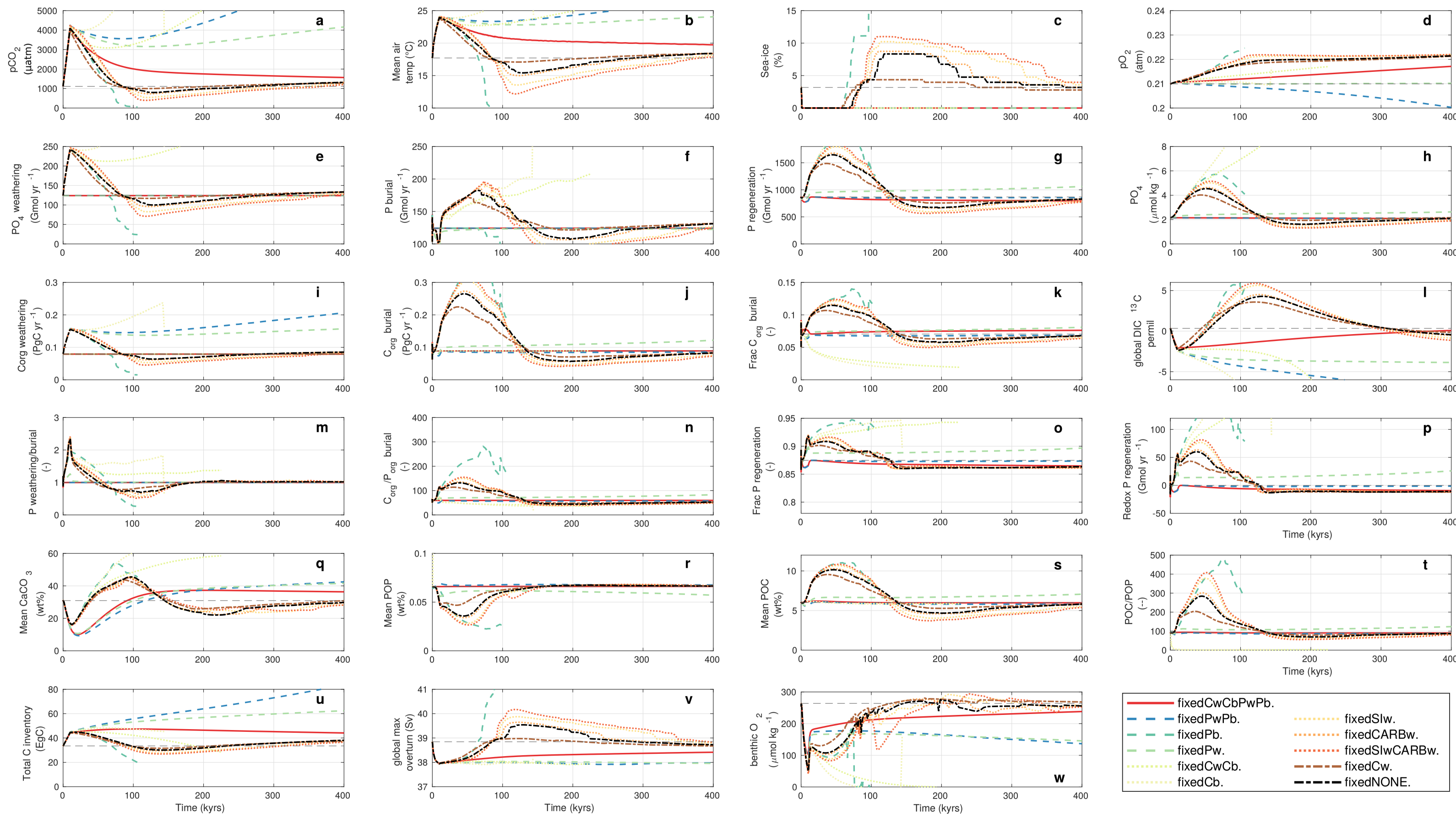

Figure S2: Time-series plots of various physical and biogeochemical state-variables and diagnostics for the perturbation simulation (CO_2 release of 10,000 PgC over 10 kyr) and the system recovery over 400 kyr for the 'feedback' experiments of Table S1. The horizontal dashed line indicates the pre-perturbation condition.

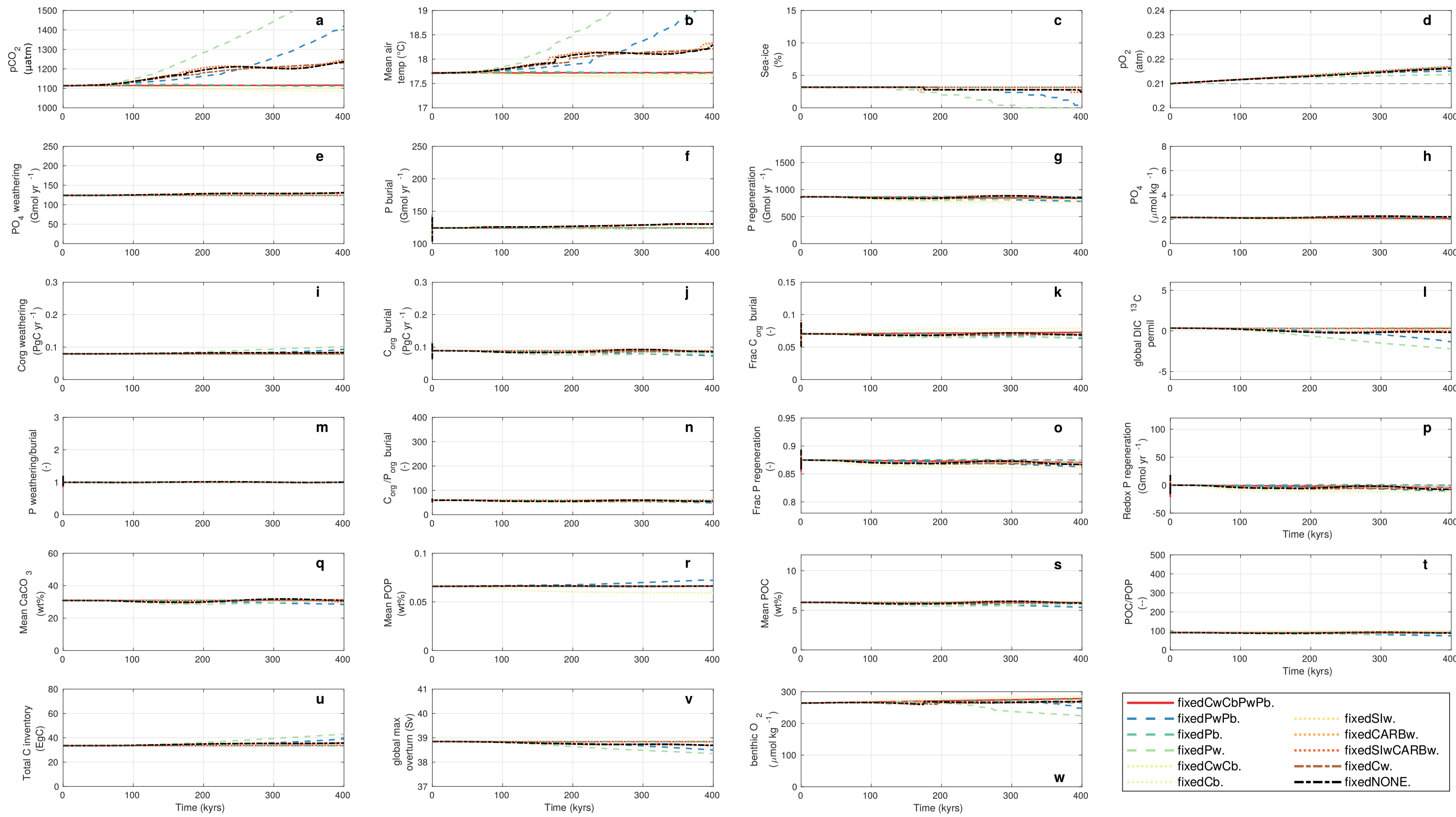

Figure S3: Time-series plots of various physical and biogeochemical state-variables and diagnostics for the control simulation (no CO_2 release) over 400 kyr for the 'feedback' experiments of Table S1.

experiment $0.6\times pO_2$ + $1.2\times PO_4^{3-}$ drives a fully ice-covered snowball state (time-series not shown). In contrast, under modern oxygen conditions and an ocean that is initialized with only $0.6\times$ modern PO_4^{3-} climate recovery is comparable to the classic silicate-weathering-only system and no over-cooling occurs (blue, dotted line, Fig. S4a and S5s).

Additional cGENIE experiments

In order to test if system dynamics are similar when using a different continental configuration, a colder (pre-industrial) climate state (i.e., 278 μatm atmospheric pCO_2), and a more elaborate representation of C_{org} burial we run an additional set of feedback experiments. We now use a continent that covers only low latitudes and features an equatorial gateway. Also this continent is surrounded by a continental shelf with a depth of $\sim$175 m and again we created a random spatial distribution of ocean depths used in the pressure-dependent calculation of calcium carbonate preservation in the sediments (Figure S7a+b).

Here C_{org} burial is simulated with the analytical diagenetic model OMEN-SED (*33*). OMEN-SED calculates benthic C_{org} burial rates by solving a vertically resolved conservation equation for solid species (e.g., (*74*)). Burial rates are primarily a function of POM settling, advection rate and the reactivity of POM. The bulk POM pool is partitioned in two reactivity classes and the degradation rate constant for the less reactive POM fraction is a function of seafloor oxygen concentration – taking a lower value for $[O_2] < 5$ μM (*75, 76*). We tuned the degradation rate constants in OMEN-SED ($k_1^{ox} = 3.5E-3$, $k_2^{ox} = 3.5E-4$, $k_2^{anox} = 3.5E-5$) to simulate a global C_{org} burial rate of 0.110 PgC yr^{-1} which is higher than in our first model setup (see Fig. S1) but still conservative considering C_{org} preservation estimates for the modern ocean (i.e., 0.09 – 0.30 PgC yr^{-1}, (*13, 57, 58, 73*)). In this configuration we simulate a global burial rate of $CaCO_3$ in deep sea sediments of 0.133 PgC yr^{-1} and a global P-burial rate of 0.10 Tmol yr^{-1}. Note that in this setup $CaCO_3$ burial is slightly larger than C_{org} burial.

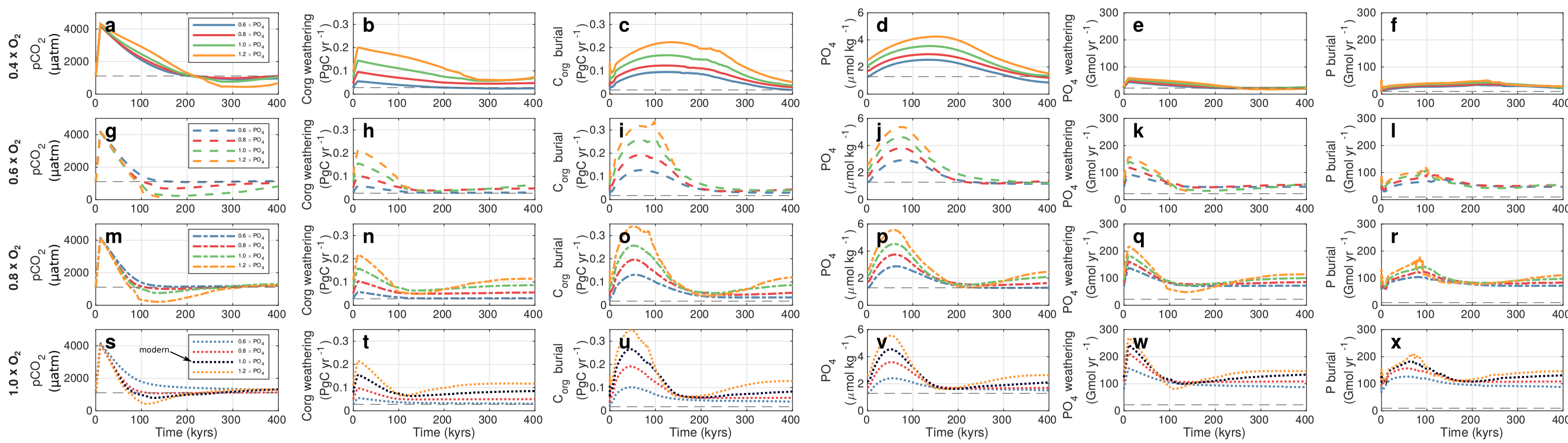

Figure S4: Time-series plots of six biogeochemical state-variables for the perturbation simulation (CO_2 release of 10,000 PgC over 10 kyr) for the 'Strengths' experiments of Table S1 separated by the initial atmospheric pO_2 conditions, i.e., (a – f) 0.4× modern, (g – l) 0.6× modern, (m – r) 0.8× modern, (s – x) 1.0× modern. For reference time-series with modern boundary conditions are plotted in black.

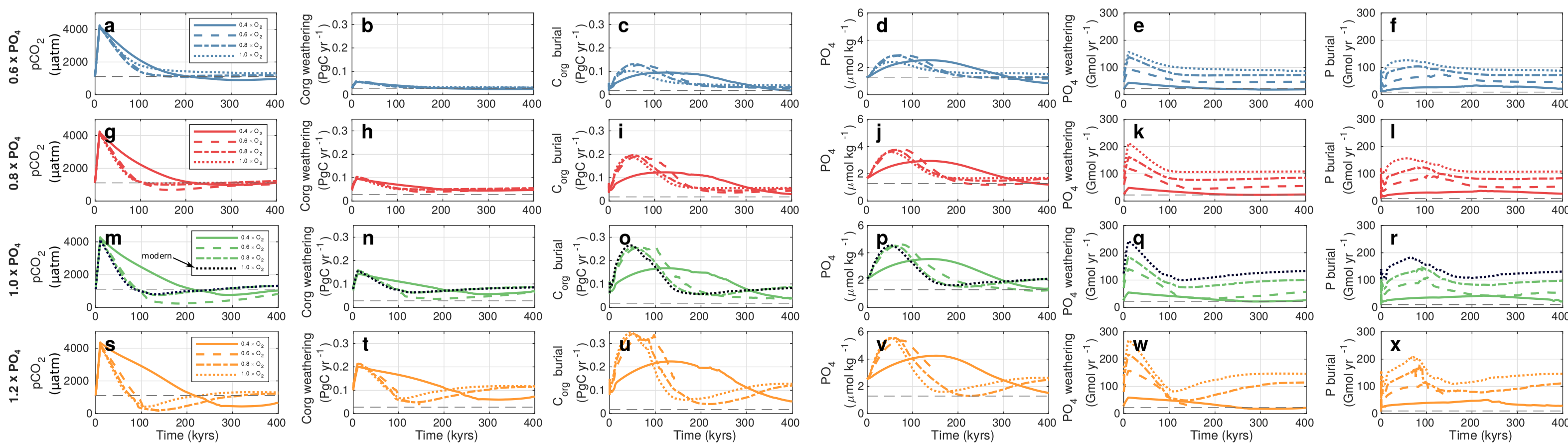

Figure S5: Time-series plots of six biogeochemical state-variables for the perturbation simulation (CO_2 release of 10,000 PgC over 10 kyr) for the 'Strengths' experiments of Table S1 separated by the initial oceanic PO_4^{3-} inventory, i.e., (a – f) 0.6× modern, (g – l) 0.8× modern, (m – r) 1.0× modern, (s – x) 1.2× modern. For reference time-series with modern boundary conditions are plotted in black.

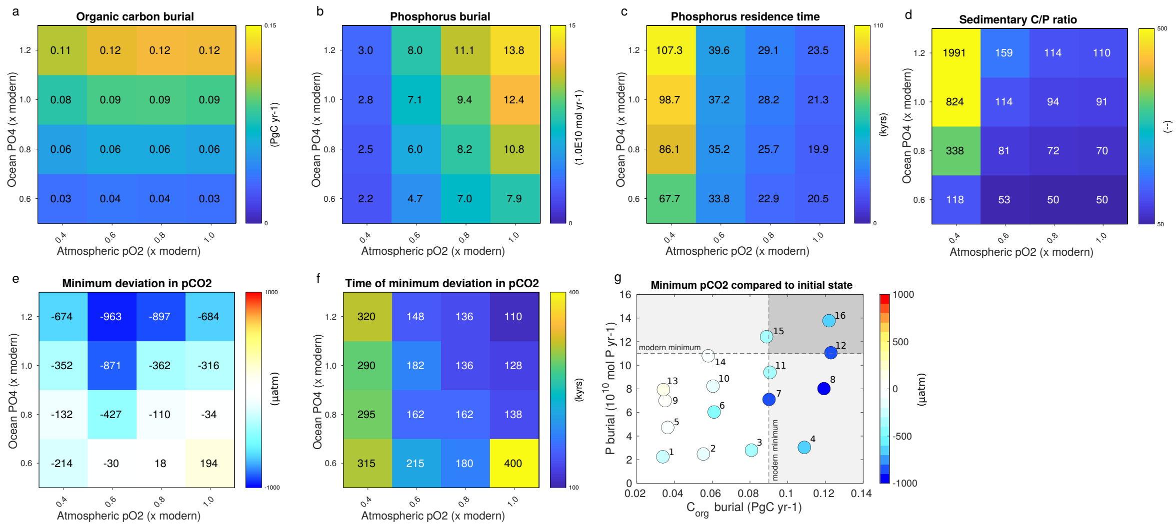

Figure S6: Analysis of the 16 'Strengths' experiments of Table S1 – similar to Fig. 3, here also including the scalar values. The P residence time is calculated for the steady-state situation at the end of SPIN2.

Although we changed main boundary conditions (i.e., continental configuration and pre-perturbation pCO_2) the general system response for the same feedback simulations (i.e., 'fixed-NONE', 'fixedCw', 'fixedPwPb', 'fixedCwCbPwPb') are comparable (compare Fig. S8 with Fig. 2). Our additional results thus indicate that the details of how the sedimentary organic matter sink responds to environmental change are not important, only that the C_{org} sink positively scales with biological productivity at the surface and P-regeneration inversely scales with seafloor oxygenation. Our additional experiments further highlight that the climate system recovers faster and over-cooling is stronger when C_{org} burial is simulated using a simple oxygen dependency (compare Fig. S8a, b, c with Fig. 2).

As in our experiments presented in Fig. 2, a rapid runaway greenhouse results if we fix P-dynamics ('fixedPwPb', Fig. S8) mainly because CO_2 release from kerogen weathering provides a positive feedback that is stronger than the negative silicate weathering and C_{org} burial feedbacks. However, our additional experiment 'fixedPwPbCw' (pink dashed line, Fig. S8),

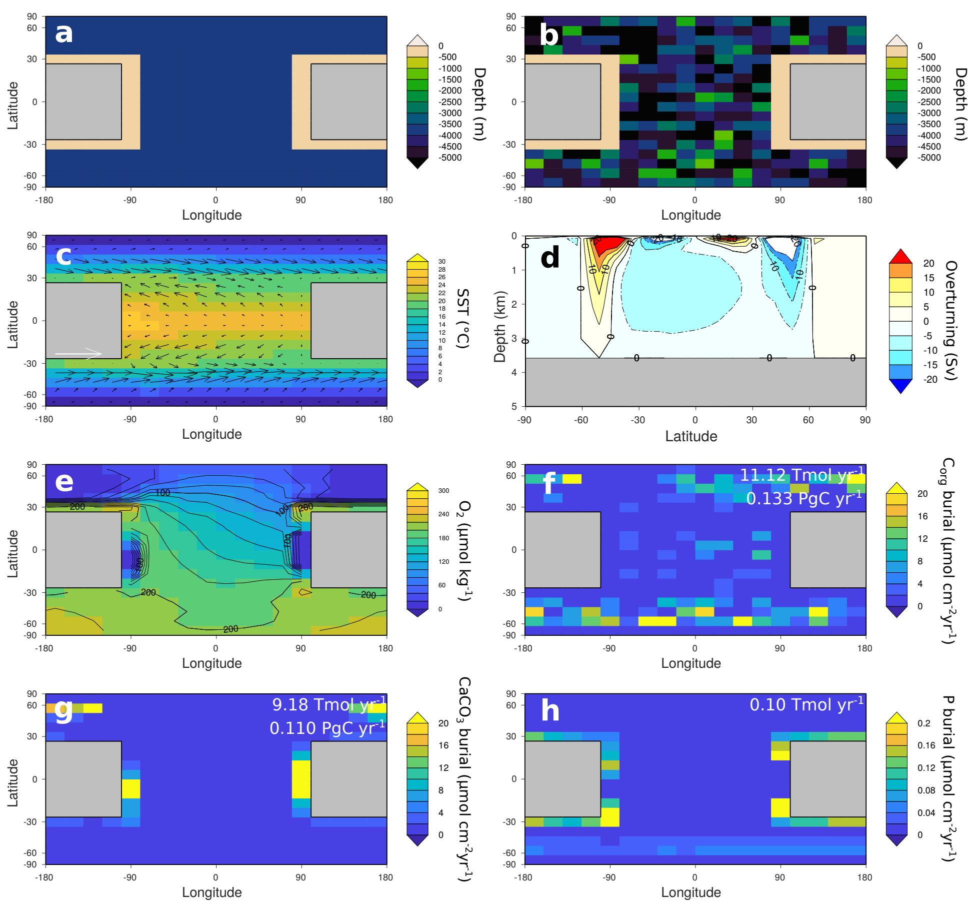

Figure S7: cGENIE configuration and equilibrium boundary conditions for the additional cGENIE experiments. **(a)** Continental configration and flat-ocean bathymetry used in the ocean circulation model. **(b)** Random spatial distribution of ocean depths used in the pressure-dependent calculation of calcium carbonate preservation in the sediments. **(c)** Simulated sea surface temperatures (SST) superimposed by vectors for ocean surface velocities, **(d)** the zonal mean ocean overturning strength, and **(e)** seafloor oxygen concentration . Burial rates of **(f)** $CaCO_3$, **(g)** organic carbon , and **(h)** phosphorus in the marine sediments. Comparable modern burial fluxes: $CaCO_3$ = 0.074 - 0.136 PgC yr^{-1} (*54–56*); organic carbon = 0.09 - 0.30 PgC yr^{-1} (*57, 58*); phosphorus = 0.11 - 0.34 Tmol yr^{-1} (*59, 60*).

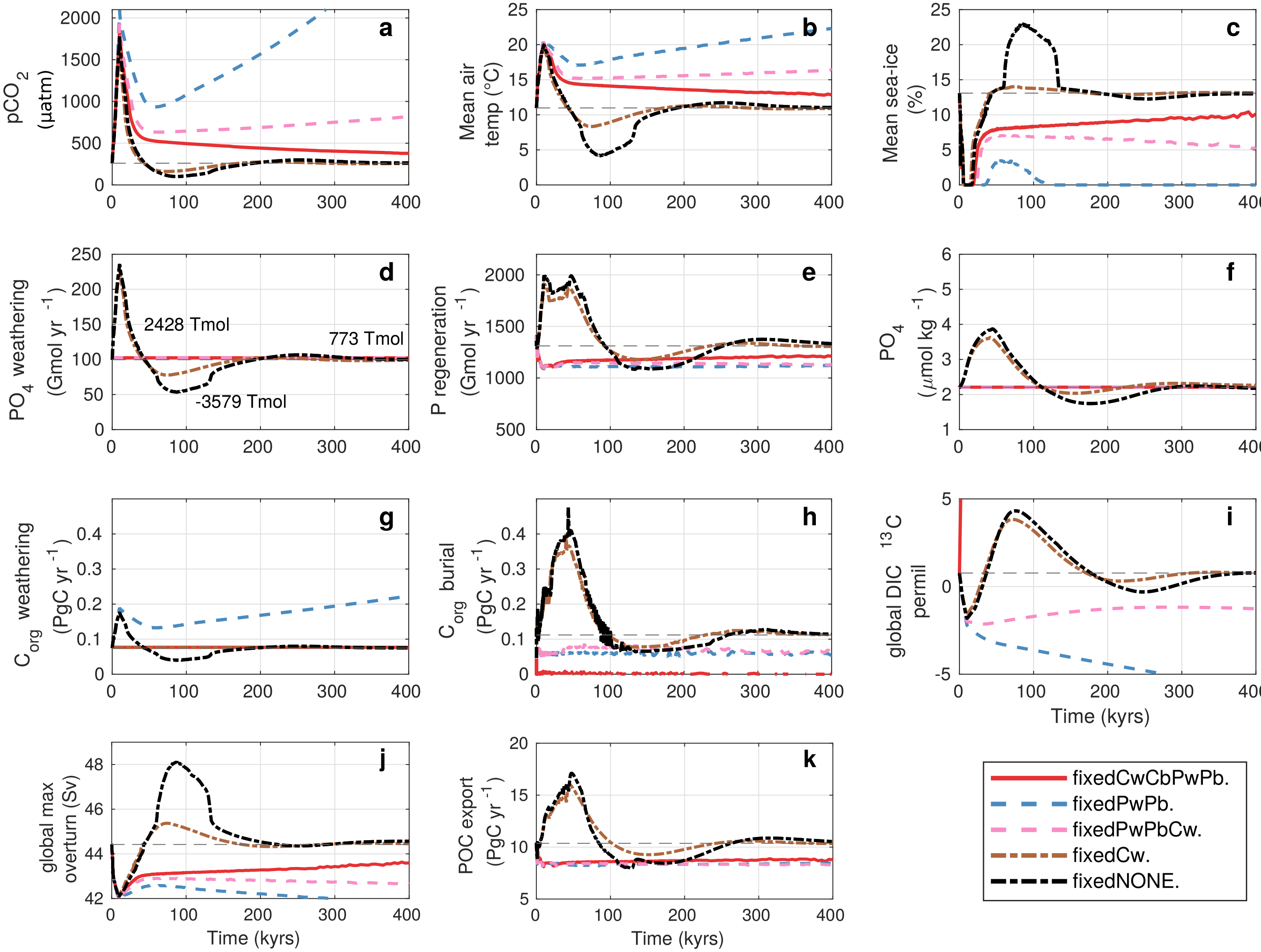

Figure S8: Time-series plots of various physical and biogeochemical state-variables and diagnostics for the perturbation simulation (CO_2 release of 10,000 PgC over 10 kyr) for five feedback experiments using OMEN-SED to calculate C_{org} burial. The horizontal dashed line indicates the pre-perturbation condition.

where we also fix the positive kerogen weathering feedback, shows that the climate system does also not recover to its pre-perturbation state (Fig. S8a, b). Responsible for this is an imbalance in C_{org} sources and sinks. Transient climate warming after the perturbation leads to reduced ocean overturning and thus nutrient availability and export productivity in the upper ocean (pink dashed lines, Fig. S8j, k). As a result, the C_{org} burial rate (Fig. S8h) is slightly lower than the steady-state C_{org} burial (and weathering) rate (grey dashed lines in Fig. S8g, h), leading to a steady increase in pCO_2 (pink dashed line, Fig. S8a). Hence, we conclude that a responsive P-cycle is a prerequisite for a recovery to the pre-perturbation climate when any type of C_{org} feedbacks are considered.